JOURNAL OF GUIDANCE, CONTROL, AND DYNAMICS
Vol. 31, No. 1, January–February 2008

Novel $\mathcal{L}_1$ Adaptive Control Methodology for Aerial Refueling with Guaranteed Transient Performance

Jiang Wang,* Vijay V. Patel,† Chengyu Cao,‡ and Naira Hovakimyan§
Virginia Polytechnic Institute and State University,
Blacksburg, Virginia 24061
and
Eugene Lavretsky¶
The Boeing Company,
Huntington Beach, California 92647

DOI: 10.2514/1.31199

Autonomous aerial refueling autopilot design is addressed in this paper using a novel $\mathcal{L}_1$ neural-network-based adaptive control approach, which is capable of accommodating trailing-vortex-induced uncertainties and uncertainties in control effectiveness. The main advantage of the new approach is its ability of fast adaptation that leads to uniform transient performance for the system's signals, both inputs and outputs, simultaneously, with guaranteed performance specifications. Simulation results verify the benefit of this new approach.

Nomenclature

$\bar{c}$	=	wing mean aerodynamic chord
g	=	gravity coefficient
h	=	vertical separation from the tanker, positive down
I_{yy}	=	moment of inertia
L_p	=	roll moment derivative due to roll rate
L_r	=	roll moment derivative due to yaw rate
L_β	=	roll moment derivative due to side-slip angle
L_{δ_a}	=	roll moment derivative due to aileron deflection
l	=	change of the relative horizontal separation, positive forward
M	=	Mach number
M_q	=	pitch moment derivative due to pitch angle
M_α	=	pitch moment derivative due to angle of attack
M_{δ_e}	=	pitch moment derivative due to elevator deflection
m	=	mass
N_p	=	yaw moment derivative due to roll rate
N_r	=	yaw moment derivative due to yaw rate
N_β	=	yaw moment derivative due to side slip
N_{δ_r}	=	yaw moment derivative due to rudder deflection
N_{δ_a}	=	yaw moment derivative due to aileron deflection
p	=	roll rate
q	=	pitch rate
S	=	wing reference area
V	=	velocity
X_q	=	drag derivative due to pitch rate
X_V	=	drag derivative due to velocity
X_α	=	drag derivative due to angle of attack
X_{δ_T}	=	thrust derivative
Y_β	=	lateral force derivative due to side-slip angle
y	=	lateral separation relative to the tanker, positive right
Z_α	=	vertical force derivative due to angle of attack
α	=	angle of attack, rad
β	=	side-slip angle, rad
γ	=	flight path angle, rad
δ_e	=	elevator deflection, deg
δ_r	=	rudder deflection, deg
δ_T	=	throttle setting
δ_a	=	aileron deflection, deg
ρ	=	density of air, slugs/ft^3
θ	=	pitch angle, rad
ϕ	=	roll angle, rad

Presented as Paper 6206 at the AIAA Guidance, Navigation, and Control Conference, Keystone, CO, 20–24 August 2006; received 22 March 2007; revision received 18 June 2007; accepted for publication 22 July 2007.

*Graduate Research Assistant, Department of Aerospace and Ocean Engineering, 215 Randolph Hall; jwang005@vt.edu. Student Member AIAA (Corresponding Author).

†Research Scientist, Department of Aerospace and Ocean Engineering, 215 Randolph Hall; vvp2069@vt.edu.

‡Research Scientist, Department of Aerospace and Ocean Engineering, 215 Randolph Hall; chengyu@vt.edu.

§Professor, Department of Aerospace and Ocean Engineering, 215 Randolph Hall; nhovakim@vt.edu. Associate Fellow AIAA.

¶Boeing Technical Fellow, Phantom Works, 5301 Bolsa Avenue, Mail Code H013-B318; eugene.lavretsky@boeing.com. Associate Fellow AIAA.

I. Introduction

WITH the advent of unmanned flight vehicles, safe and reliable autonomous aerial refueling (AAR) capabilities become a necessity. Reference [1] presents a good overview of the challenges involved in autonomous aerial refueling. Two aerial refueling procedures, the probe-and-drogue method and the boom-receptacle method, are being employed by the U.S. Navy/NATO and the U.S. Air Force, respectively. The boom-receptacle refueling procedure requires a special tanker and human operator onboard, and the workload of the receiver aircraft is less than that of the probe-and-drogue approach. On the contrary, the probe-and-drogue refueling procedure does not need a special tanker and/or human operator in the loop, but it requires a good autonomous tracking controller. This has proven to be extremely difficult due to the aerodynamic coupling among the two aircraft and the drogue. The autopilot has to compensate for the uncertainties due to the trailing vortices of the tanker when the receiver is flying from the observation point to the contact point. The method proposed in this paper achieves this control objective with a uniformly bounded transient response. It can be also equally applied for the boom-receptacle method employed for aerial refueling.

Aerial refueling has been intensively addressed over the past decades from various perspectives [1–20]. Several methods,

combined with various sensors, have been practiced for obtaining accurate measurements of the drogue, such as use of a global positioning system (GPS) [2,9], visual servoing with pattern recognition [3,4,11], and vision-based navigation systems [13,14]. A GPS-based sensor has been used with machine-vision-based sensors to achieve accurate positioning and capturing [8]. In [6], a new set of nonlinear equations of motion are derived, including the relative motion of the receiver and the tanker and the aerodynamic coupling due to the trailing vortex of the tanker. Vortex-effect modeling is developed in [5,15]. Proportional–integral–derivative control laws for each of the three position-separation axes are used in [16] without considering the effect of the trailing vortex in the simulation. Quantitative feedback theory was applied to take care of the wind gust and fuel-transferring disturbances [10]. In [18], the authors studied the applicability of proportional navigation guidance and line-of-sight angle control in aerial refueling, using a turbulence model instead of modeling the vortex-induced effect. An optimal nonzero set point with a control-rate-weighting controller was applied to track and dock with a stationary drogue under the influence of Dryden light turbulence [13]. Reference [14] developed a reference-observer-based tracking controller.

The trailing-vortex-induced wind field presents a significant challenge from a control design perspective. The situation is also complicated by the fact that the modeling of the vortex effect is far from satisfactory. This brings up the idea of implementing model reference adaptive control (MRAC) architecture with neural networks [12], which requires less a priori knowledge of the trailing-vortex effect. However, in such uncertain dynamic environments, the transient performance of MRAC can be unpredictable [21]. A novel $\mathcal{L}_1$ neural network adaptive control method is considered in this paper for solving the AAR problem [22–25]. The benefit of this new adaptive architecture is its capability for fast adaption that leads to the desired transient response in addition to stable tracking for the system's input and output signals simultaneously. It has systematic design methodology to guarantee performance specifications along with stability margins [22–24,26–28].

This paper extends the work of [29] to accommodate uncertainties in control effectiveness such as actuator failures. In this paper, the probe-and-drogue aerial refueling system is considered for the linearized six-degree-of-freedom (6-DOF) model of the aircraft under the assumption that the drogue coordinates are measured with sufficient accuracy. The autopilot design aims at achieving automatic maneuvers of the receiver aircraft (manned or unmanned) to send the probe to the close proximity of the moving drogue. The coordinates of the drogue can be considered as reference inputs that the receiver aircraft needs to track with prespecified precision in finite time.

The paper is organized as follows. In Sec. III, we give the problem formulation. In Sec. IV, we introduce the aircraft model and the wake model. Section V presents an overview of the novel $\mathcal{L}_1$ adaptive control architecture. Section VI discusses the performance bounds of this architecture. Simulation results for an unmanned aerial refueling aircraft model are presented in Sec. VII.

II. Problem Formulation

We consider a decoupled 6-DOF aircraft model for the refueling aircraft. We assume that both the receiver and the tanker aircraft are in straight and level flight in the beginning of the maneuver. We will assume that during the entire aerial refueling maneuver the receiver aircraft is subject only to small perturbations so that the linearized decoupled dynamics can be used to describe its motion with some level of fidelity, with additive uncertainties coming from the trailing vortices induced by the tanker aircraft. For the aerial refueling maneuver all angles can be assumed small. Subject to these assumptions, and neglecting the influence of gravity, thrust, and elevator on the angle of attack, the 6-DOF aircraft dynamics can be described as

$$
\begin{aligned}
\dot{l} &= V \\
\dot{V} &= X_V V - g\theta + X_q q + X_\alpha \alpha + X_{\delta_T}\Lambda_1(\delta_{T_{\text{in}}} + \delta_T) + \Delta_1(l,h,y) \\
\dot{\alpha} &= q + \frac{Z_\alpha}{V_0}\alpha, \qquad \dot{\theta} = q \\
\dot{q} &= M_q q + M_\alpha \alpha + M_{\delta_e}\Lambda_2(\delta_{e_{\text{in}}} + \delta_e) + \Delta_2(l,h,y) \\
\dot{h} &= V_0(\theta - \alpha), \qquad \dot{\phi} = \frac{\cos\gamma_0}{\cos\theta_0}p + \frac{\sin\gamma_0}{\cos\theta_0}r \\
\dot{\beta} &= \frac{g\cos\theta_0}{V_0}\phi + \frac{Y_\beta}{V_0}\beta - r \\
\dot{p} &= L_\beta\beta + L_p p + L_r r + L_{\delta_a}\Lambda_3(\delta_{a_{\text{in}}} + \delta_a) + L_{\delta_r}\delta_{r_{\text{in}}} + \Delta_3(l,h,y) \\
\dot{r} &= N_\beta\beta + N_p p + N_r r + N_{\delta_r}\delta_{r_{\text{in}}} + N_{\delta_a}(\delta_{a_{\text{in}}} + \delta_a) \\
\dot{y} &= Y_\phi\phi + V_0\beta
\end{aligned} \tag{1}
$$

where $\Delta_1(l,h,y)$, $\Delta_2(l,h,y)$, and $\Delta_3(l,h,y)$ are the wake-induced incremental changes to the horizontal acceleration, the pitch-angle acceleration, and the roll-angle acceleration, respectively. The coefficients $0 < \Lambda_i \le 1$ $(i = 1, 2, 3)$ model the reduction in control effectiveness. The receiver dynamics are trimmed around V_0, α_0, and θ_0, and the tanker is assumed to be trimmed for straight and level flight with the same trim conditions. The coordinate system is the body-fixed system of the tanker aircraft. In Eq. (1), $\delta_{T_{\text{in}}}$, $\delta_{e_{\text{in}}}$, $\delta_{a_{\text{in}}}$, and $\delta_{r_{\text{in}}}$ are the inner-loop controllers, which are designed via proportional–integral feedback to keep θ, α, q, V, β, ϕ, p, and r close to the trim conditions. We note that the inner-loop stabilization can be achieved via any of the conventional linear design methods (see, for example, [30]) and is not elaborated in this paper for the sake of brevity. We will focus on the design of the outer-loop controllers δ_T, δ_e, δ_a, and δ_r to enable the aerial refueling maneuver in the highly uncertain dynamic environment. With the inner-loop stabilization, the equations of motion can be expressed as

$$
\begin{aligned}
\dot{l} &= V, \qquad \dot{V} = X'_V V + X_{\delta_T}\Lambda_1\delta_T + \Delta_1(l,h,y) \\
\dot{\alpha} &= q + \frac{Z_\alpha}{V_0}\alpha, \qquad \dot{\theta} = q \\
\dot{q} &= M'_q q + M'_\alpha \alpha + M_{\delta_e}\Lambda_2\delta_e + \Delta_2(l,h,y), \qquad \dot{h} = V_0(\theta - \alpha) \\
\dot{\phi} &= \frac{\cos\gamma_0}{\cos\theta_0}p + \frac{\sin\gamma_0}{\cos\theta_0}r, \qquad \dot{\beta} = \frac{g\cos\theta_0}{V_0}\phi + \frac{Y_\beta}{V_0}\beta - r \\
\dot{p} &= L'_\beta\beta + L'_p p + L'_r r + L_{\delta_a}\Lambda_3\delta_a + \Delta_3(l,h,y) \\
\dot{r} &= N'_\beta\beta + N'_p p + N'_r r, \qquad \dot{y} = Y_\phi\phi + V_0\beta
\end{aligned} \tag{2}
$$

where X'_V, M'_q, M'_α, L'_β, L'_p, L'_r, N'_β, N'_p, and N'_r are the redefined coefficients due to the proportional feedback used for inner-loop stabilization. Usually, for the lateral axis, the inner-loop control is designed using an aileron-to-rudder interconnect to achieve stability-axis roll without generating slide slip or yaw rate, which consequently reduces the term N_{δ_a} to zero, and therefore it has been neglected in Eq. (2).

The preceding set of equations of motion can be divided into three subsystems that can be written in state-space form as

$$
\begin{aligned}
\dot{X}_i(t) &= A_i X_i(t) + B_i\{\Lambda_i u_i(t) + \Delta_i[Y(t)]\}, \qquad X_i(0) = X_{i0} \\
Y_i(t) &= c_i^\top X_i(t)
\end{aligned} \tag{3}
$$

where $i = 1, 2, 3$, $X(t) = [X_1^\top(t) \;\; X_2^\top(t) \;\; X_3^\top(t)]^\top$, and

$$
Y(t) = [Y_1(t) \;\; Y_2(t) \;\; Y_3(t)]^\top = [l(t) \;\; h(t) \;\; y(t)]^\top
$$

is the regulated output of interest for the aerial refueling. Furthermore, $A_i \in \mathbb{R}^{n_i \times n_i}$, $B_i \in \mathbb{R}^{n_i \times 1}$, $c_i \in \mathbb{R}^{n_i \times 1}$, u_i, Λ_i, and $\Delta_i \in \mathbb{R}$. We also assume that some conservative knowledge of $\Lambda_u > \Lambda_l > 0$ is available such that $\Lambda_i \in [\Lambda_l, \Lambda_u]$.

The first subsystem uses the thrust input to control the horizontal separation. Its states, system matrices, and control input are

$$X_1 = \begin{bmatrix} l \\ V \end{bmatrix}, \qquad A_1 = \begin{bmatrix} 0 & 1 \\ 0 & X'_V \end{bmatrix}, \qquad B_1 = \begin{bmatrix} 0 \\ 1 \end{bmatrix}$$
$$c_1 = \begin{bmatrix} 1 \\ 0 \end{bmatrix}, \qquad u_1 = X_{\delta_T}\delta_T \tag{4}$$

The second subsystem uses the elevator input to control the vertical separation. Its states, system matrices, and control input are

$$X_2 = \begin{bmatrix} \alpha \\ \theta \\ q \\ h \end{bmatrix}, \qquad A_2 = \begin{bmatrix} \frac{Z_\alpha}{V_0} & 0 & 1 & 0 \\ 0 & 0 & 1 & 0 \\ M_\alpha & 0 & M_q & 0 \\ -V_0 & V_0 & 0 & 0 \end{bmatrix}$$
$$B_2 = \begin{bmatrix} 0 \\ 0 \\ 1 \\ 0 \end{bmatrix}, \qquad c_2 = \begin{bmatrix} 0 \\ 0 \\ 0 \\ 1 \end{bmatrix}, \qquad u_2 = M_{\delta_e}\delta_e \tag{5}$$

The third subsystem is used to control the lateral separation with the aileron input. Its states, system matrices, and control input are

$$X_3 = \begin{bmatrix} \phi \\ \beta \\ p \\ r \\ y \end{bmatrix}, \qquad A_3 = \begin{bmatrix} 0 & 0 & \frac{\cos\gamma_0}{\cos\theta_0} & \frac{\sin\gamma_0}{\cos\theta_0} & 0 \\ \frac{g\cos\theta_0}{V_0} & \frac{Y_\beta}{V_0} & 0 & -1 & 0 \\ 0 & L_\beta & L_p & L_r & 0 \\ 0 & N_\beta & N_p & N_r & 0 \\ Y_\phi & V_0 & 0 & 0 & 0 \end{bmatrix}$$
$$B_3 = \begin{bmatrix} 0 \\ 0 \\ 1 \\ 0 \\ 0 \end{bmatrix}, \qquad c_3 = \begin{bmatrix} 0 \\ 0 \\ 0 \\ 0 \\ 1 \end{bmatrix}, \qquad u_3 = M_{\delta_a}\delta_a \tag{6}$$

From experimental evaluation, some conservative knowledge can be extracted about the growth rate of the uncertainties $\Delta_i(Y)$, so that one has the following uniform bounds over some compact set $Y \in \mathcal{D}_i$:

$$|[\Delta_i(Y') - \Delta_i(Y'')]| \le L_{w_i}\|Y' - Y''\|$$
$$Y', Y'' \in \mathcal{D}_i, \qquad \max_{i=1,2,3}|\Delta_i(0)| \le B_{0_i} \tag{7}$$

where $i = 1, 2, 3$, $L_{w_i} > 0$ and B_{0_i} are known, and the set $\mathcal{D}_i$ will be subsequently specified.

The control objective is to fly the receiver aircraft into a prescribed neighborhood of the drogue center within a prescribed finite time interval. Thus, denoting the drogue's center coordinates by

$$Y_{\text{cmd}}(t) = [x_d(t) \;\; y_d(t) \;\; z_d(t)]^\top$$

in the tanker body-fixed coordinate frame, the refueling can start at any time instant $t' \le T_f$, if $|x(t') - x_d(t')| < \delta_d$ and

$$\|[y(t') \;\; z(t')]^\top - [y_d(t') \;\; z_d(t')]^\top\|_2 \le r_d$$

where r_d is the radius of the drogue, δ_d is a small positive number, T_f is the prescribed time within which the probe needs to contact the drogue, and $\|\cdot\|_2$ denotes the 2-norm.

The main challenge of the aerial refueling problem is associated with the precise position control of the receiver aircraft within the prescribed finite time T_f in the presence of uncertain nonlinear aerodynamic wake effects caused by the airflow behind the tanker and possible loss of control effectiveness. The finite time requirement in such dynamic uncertain environment implies that the proposed method for the autopilot design needs to have guaranteed transient performance. Let the transient performance specifications for such a maneuver be given by a strictly proper and stable transfer function $H(s)$ that ensures the required finite time-to-contact. Thus, the autopilot needs to ensure that in the presence of wake-induced uncertainties,

$$Y(s) \approx H(s)Y_{\text{cmd}}(s)$$

where $Y(s)$ and $Y_{\text{cmd}}(s)$ are the Laplace transformation of $Y(t)$ and $Y_{\text{cmd}}(t)$, respectively.

III. Aircraft Model and Wake Modeling

A. Unmanned Aerial Vehicle Model

The control design is applied to a linearized 6-DOF flying-wing unmanned aerial vehicle (UAV) model, known as the Barron Associates nonlinear tailless aircraft model (BANTAM) [31]. This medium-fidelity model was developed primarily using the data from [32] and the analytical estimates of dynamic stability derivatives from DATCOM and HASC-95. The aircraft is statically unstable at low angles of attack. It has two pairs of body flaps mounted on the trailing edge of the wing, and a pair of spoilers is mounted upstream of the flaps. The geometry of BANTAM is shown in Fig. 1. The conventional elevator, aileron, and rudder control inputs need to be

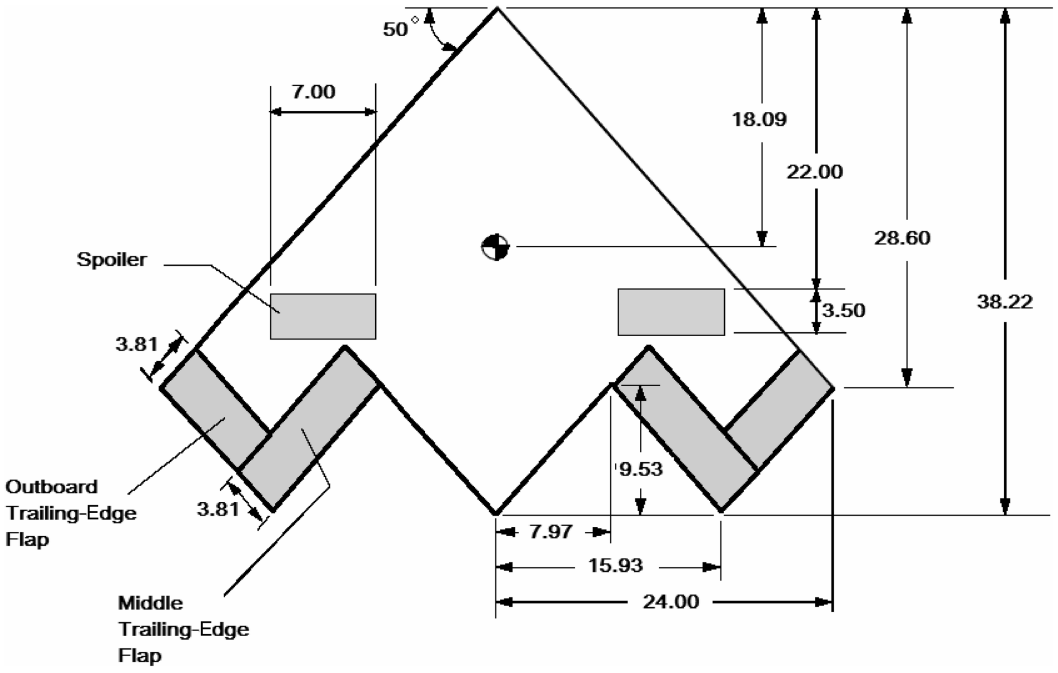

Fig. 1 BANTAM configuration.

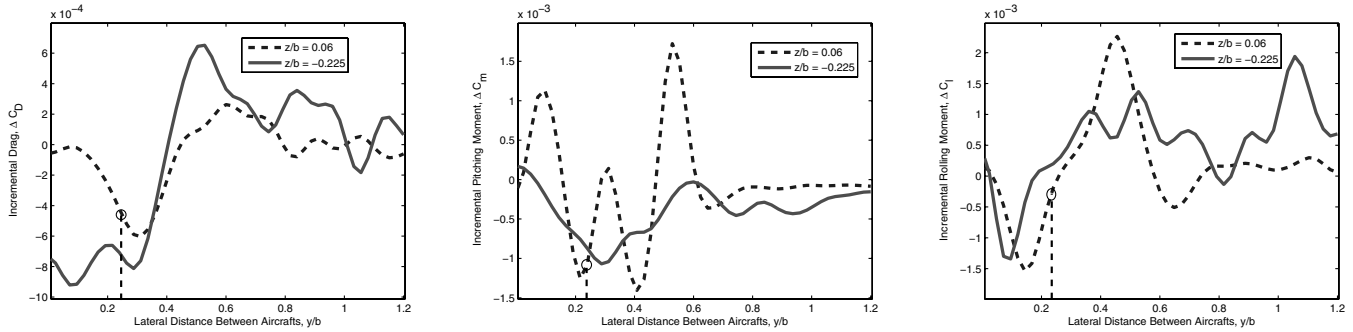

Fig. 2 Wake-induced drag, pitch moment, and roll moment coefficients.

transformed into appropriate commands to flaps and spoilers (through some type of control allocation scheme). The flaps provide the functions for both elevator and aileron. The spoilers move asymmetrically to generate yaw authority, and their symmetrical motion generates drag.

B. Wake Modeling

The wake-effect data are taken from a wind-tunnel test of a delta wing UAV behind a KC-135R tanker [5]. The experiment was conducted to collect the data necessary to model the effects of the wake of a KC-135R tanker on the aerodynamics of a similar-scale UAV-like aircraft (in ICE101 configuration) in a refueling scenario. The effects of the wake on the receiver aircraft vary more significantly with the change in the relative lateral and vertical positions, compared with the relative horizontal position. The wake effects change the aerodynamic force and moment coefficients of the receiver aircraft. From the measured data, this experiment creates the incremental coefficients change (lift, drag, side force, pitching moment, rolling moment, and yaw moment coefficients) as functions of three directions (longitudinal, lateral, and vertical separations). Our adaptive control design focuses on compensation of the uncertainties caused by three significantly changing coefficients: those of rolling moment, pitching moment, and drag.

To show the aerodynamic force and moment coefficients variations with respect to separation changes, parts of the data are plotted in Fig. 2. The horizontal, vertical, and lateral separations are expressed in a normalized way: divided by the wing span b of the tanker. In each subplot, the incremental change of the aerodynamic coefficients vs the lateral separation variation is plotted for two different vertical separation distances: $z/b = 0.06$ and $z/b = -0.225$. In all cases, the horizontal separation between the receiver aircraft and the tanker remains constant. This distance, measured from the center of gravity of the receiver to that of the tanker, is 110.5 ft, which corresponds to the closest horizontal separation in the experiment. Vertical separation $z/b = 0.06$ corresponds to the vertical distance from the origin of the drogue position. In the plots, the drogue position is shown by a circle, and at that particular position, the increment of the drag is 388.6 lbf, the increment of the pitching moment is $19,036$ lbf $\cdot$ ft, and the increment of the rolling moment is $10,720$ lbf $\cdot$ ft.

From the plots, it also can been seen that when the receiver changes its relative separation with respect to the tanker vertically and laterally, the aerodynamic coefficients vary drastically. Thus, as the receiver approaches the drogue, the wake vortex can deteriorate the receiver's performance, creating a challenge for achieving the finite prescribed time to contact.

IV. Autopilot Design for Aerial Refueling

To develop a robust and reliable autopilot, we need first to make sure that in the absence of the wake, the linearized decoupled dynamics are properly stabilized by some type of linear controller so that adaptive augmentation will be used purely for compensation of the wake-induced uncertainties.

A. Outer-Loop Feedback Structure and the Closed-Loop System

The outer loop is stabilized via state feedback linear quadratic regulator (LQR) and integral control. For each of the subsystems (3), the controller is designed to achieve stabilization in the absence of the wake effects and loss of control effectiveness. We first rewrite the single-input/single-output system in Eq. (3) when $\Lambda_i = 1$ and $\Delta_i = 0$ as

$$\dot{X}_i(t) = A_i X_i(t) + B_i u_i(t), \qquad X_i(0) = X_{i0}, \qquad Y_i(t) = c_i^\top X_i(t) \tag{8}$$

where $i = 1, 2, 3$. We introduce the integral error as

$$y_I(t) = \int_0^t [Y_i(\tau) - Y_{\mathrm{cmd}_i}(\tau)]\,\mathrm{d}\tau$$

Augmented with these additional states, the system dynamics in Eq. (8) take the form

$$\begin{bmatrix} \dot{X}_i \\ \dot{y}_I \end{bmatrix} = \underbrace{\begin{bmatrix} A_i & 0 \\ c_i^\top & 0 \end{bmatrix}}_{\mathcal{A}_i} \underbrace{\begin{bmatrix} X_i \\ y_I \end{bmatrix}}_{x_i} + \underbrace{\begin{bmatrix} B_i \\ 0 \end{bmatrix}}_{\mathcal{B}_i} u_i + \begin{bmatrix} 0 \\ -1 \end{bmatrix} Y_{\mathrm{cmd}_i} \tag{9}$$

$$Y_i(t) = c_i^\top X_i(t) \tag{10}$$

where $i = 1, 2, 3$. The controller $u_i(t)$ is chosen in each subsystem to have the form

$$u_i(t) = \Big[\underbrace{-k_{I_i} y_I(t) - k_{P_i} X_i(t)}_{u_{\mathrm{lin}_i}(t)} + u_{\mathrm{ad}_i}(t)\Big] \tag{11}$$

where $u_{\mathrm{lin}_i}(t)$ is the baseline linear controller for the ith channel, and $u_{\mathrm{ad}_i}(t)$ is the adaptive augmentation. Using LQR, the state feedback gains $K_i = -[k_{I_i} \;\; k_{P_i}]$ can be obtained to minimize the cost function

$$J_i = \int_0^\infty \left\{ \begin{bmatrix} X_i^\top y_I \end{bmatrix} \mathbb{Q}_i \begin{bmatrix} X_i^\top y_I \end{bmatrix}^\top + u_{\mathrm{lin}_i}^2 \mathbb{R}_i \right\} \mathrm{d}t$$

where $\mathbb{Q}_i$ and $\mathbb{R}_i$ are the design parameters of the LQR for each subsystem.

Then the closed-loop system has the following structure:

$$\begin{bmatrix} \dot{X}_i \\ \dot{y}_I \end{bmatrix} = \underbrace{[\mathcal{A}_i + \mathcal{B}_i K_i]}_{A_{m_i}} \underbrace{\begin{bmatrix} X_i \\ y_I \end{bmatrix}}_{x_i} + \underbrace{\begin{bmatrix} 0 \\ -1 \end{bmatrix}}_{B_{m_i}} \underbrace{[\,Y_{\mathrm{cmd}_i}(t)\,]}_{\mathcal{R}_i(t)} + \mathcal{B}_i u_{\mathrm{ad}_i}$$

which consequently reduces the closed-loop system for the ith channel to the following compact form:

$$\begin{aligned} \dot{x}_i(t) &= A_{m_i} x_i(t) + \mathcal{B}_i u_{\mathrm{ad}_i}(t) + B_{m_i} \mathcal{R}_i(t) \\ x_i(0) &= x_{i_0}, \qquad Y_i(t) = c_i^\top X_i(t) \end{aligned} \tag{12}$$

The choice of the feedback gains k_{P_i} and k_{I_i} needs to ensure that the linear closed-loop system has the desired response in the absence

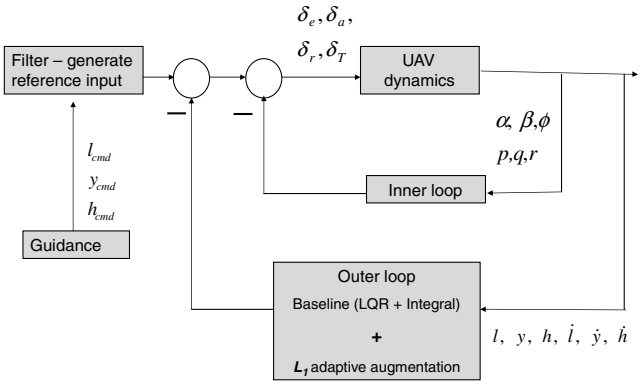

Fig. 3 Controller structure block diagram.

of wake-induced uncertainties and without any loss of control effectiveness with reasonable stability margins. The baseline controller is designed in a decoupled way; that is, pitch stick δ_e is used for the vertical axis, roll stick δ_a is used for the lateral axis, and throttle command δ_T is used for the horizontal axis. The block diagram in Fig. 3 shows the structure of the overall controller.

B. $\mathcal{L}_1$ Adaptive Control Design

In this section, we present the $\mathcal{L}_1$ adaptive control architecture from [22–24], which adapts fast leading to desired transient performance for the system's control signals and states simultaneously. Thus, it provides a suitable architecture for solving the AAR problem. The dynamics for the ith channel can be written as

$$\dot{x}_i(t) = (\mathcal{A}_i + \mathcal{B}_i\Lambda_i K_i)x_i(t) + \mathcal{B}_i\{\Lambda_i u_{\mathrm{ad}_i}(t) + \Delta_i[Y(t)]\} + B_{m_i}\mathcal{R}_i(t)$$
$$x_i(0) = x_{i_0}, \quad Y_i(t) = c_i^\top X_i(t) \tag{13}$$

Following Eq. (13) and taking into consideration that $A_{m_i} = \mathcal{A}_i + \mathcal{B}_i K_i$, we have

$$\dot{x}_i(t) = A_{m_i}x_i(t) + B_{m_i}\mathcal{R}_i(t) + \mathcal{B}_i\Big[\Lambda_i u_{\mathrm{ad}_i}(t) + \Delta_i[Y(t)] + k_{x_i}^\top x_i(t)\Big] \tag{14}$$

where

$$k_{x_i}^\top = (\Lambda_i - 1)K_i \tag{15}$$

We consider linear parametrization of the system uncertainties $\Delta_i(Y)$ over a compact set by a neural network:

$$\Delta_i(Y) = w_i^\top\Phi_i(Y) + \epsilon_i(Y), \qquad \|\epsilon_i(Y)\| \le \epsilon_i^*, \qquad Y \in \mathcal{D}_i \tag{16}$$

where $\Phi_i(Y)$ is a vector of suitably chosen Gaussian basis functions of dimension $p_i \times 1$, $w_i \in \mathbb{R}^{p_i\times 1}$ is a vector of constant unknown weights, and ϵ_i^* is the uniform bound for the approximation error over the set $\mathcal{D}_i$ that will be specified shortly. The ith element $\Phi_i(Y)$ is defined as

$$\Phi_i(Y) = \exp\left(-\frac{(Y-\kappa_i)^\top(Y-\kappa_i)}{\vartheta_i^2}\right)$$

in which the parameters κ_i and ϑ_i are the prefixed centers and widths. We consider the following state predictor:

$$\dot{\hat{x}}(t) = A_{m_i}\hat{x}(t) + B_{m_i}\mathcal{R}_i(t) + \mathcal{B}_i\Big[\hat{\Lambda}_i(t)u_{\mathrm{ad}_i}(t) + \hat{k}_{x_i}^\top(t)x_i(t) + \hat{w}_i^\top(t)\Phi_i(Y)\Big] \tag{17}$$

in which $\hat{\Lambda}_i(t)$, $\hat{k}_{x_i}(t)$, $\hat{w}_i(t)$ are the adaptive parameters. The adaptive laws are

$$\dot{\hat{\Lambda}}_i(t) = \Gamma\mathrm{proj}[\hat{\Lambda}_i(t), -u_{\mathrm{ad}_i}(t)\tilde{x}_i^\top(t)P\mathcal{B}_i]$$
$$\dot{\hat{k}}_{x_i}(t) = \Gamma\mathrm{proj}[\hat{k}_{x_i}(t), -x_i(t)\tilde{x}_i^\top(t)P\mathcal{B}_i] \tag{18}$$
$$\dot{\hat{w}}_i(t) = \Gamma\mathrm{proj}[\hat{w}_i(t), -\Phi_i[Y(t)]\tilde{x}_i^\top(t)P\mathcal{B}_i]$$

in which $\tilde{x}(t) = \hat{x}(t) - x(t)$ is the tracking error between the system dynamics in Eq. (13) and the state predictor (17), $\Gamma > 0$ is the adaptations gain, and $P = P^\top > 0$ is the solution of the algebraic Lyapunov equation $A_{m_i}^\top P_i + P_i A_{m_i} = -Q_i$, $Q > 0$, and $\mathrm{proj}(\cdot,\cdot)$ denotes the projection operator [33] (see the Appendix for the definition and properties).

The control signal is generated through gain feedback of the following system:

$$\chi_i(s) = D_i(s)r_{u_i}(s), \qquad u_{\mathrm{ad}_i}(s) = -k_i\chi_i(s), \qquad k_i > 0 \tag{19}$$

where $r_{u_i}(s)$ is the Laplace transformation of $r_{u_i}(t) = \hat{\Lambda}_i(t)u_{\mathrm{ad}_i}(t) + \bar{r}_i(t)$,

$$\bar{r}_i(t) = \hat{k}_{x_i}^\top(t)x_i(t) + \hat{w}_i^\top(t)\Phi[Y(t)] \tag{20}$$

and $D_i(s)$ is any transfer function that leads to a strictly proper stable

$$C_i(s) = \frac{\Lambda_i k_i D_i(s)}{1 + \Lambda_i k_i D_i(s)}$$

where $i = 1, 2, 3$, with low-pass gain $C_i(0) = 1$. The design parameter k_i will be introduced shortly. One simple choice for $D_i(s)$ is

$$D_i(s) = \frac{1}{s} \tag{21}$$

which yields a first-order strictly proper $C_i(s)$ in the following form:

$$C_i(s) = \frac{\Lambda_i k_i}{s + \Lambda_i k_i} \tag{22}$$

Further, let

$$L_{x_i} = \max\{|\Lambda_l - 1|, |\Lambda_u - 1|\}\|K_i\|_{\mathcal{L}_1} \tag{23}$$

We now state the $\mathcal{L}_1$ performance requirement that ensures stability of the entire system and desired transient performance, as in [22].

Design $D_i(s)$ and k_i to satisfy

$$\|\bar{G}_i(s)\|_{\mathcal{L}_1}L_i < 1 \tag{24}$$

where

$$L_i = L_{w_i} + L_{x_i} \tag{25}$$

$$\bar{G}_i(s) = (s\mathbb{I} - A_{m_i})^{-1}\mathcal{B}_i[1 - C_i(s)] \tag{26}$$

in which L_{w_i} and L_{x_i} are defined in Eqs. (7) and (23).

Because the performance results are always local with radial basis function (RBF) approximation, one needs to characterize the set $\mathcal{D}_i$ on which the RBFs are distributed. Let

$$\mathcal{D}_i = \{x_i | \|x_i\|_\infty \le \gamma_{r_i} + \gamma_{1_i} + \gamma_{0_i} + \sigma_i\} \tag{27}$$

where $\sigma_i > 0$ is an arbitrary positive constant, and

$$\gamma_{r_i} = \frac{\|H_{m_i}(s)\|_{\mathcal{L}_1}\|\mathcal{R}_i\|_{\mathcal{L}_\infty} + \|\bar{G}_i(s)\|_{\mathcal{L}_1}(B_{0_i} + \epsilon_i^*) + \|H_{o_i}(s)\|_{\mathcal{L}_1}\epsilon_i^*}{1 - \|\bar{G}_i(s)\|_{\mathcal{L}_1}L} \tag{28}$$

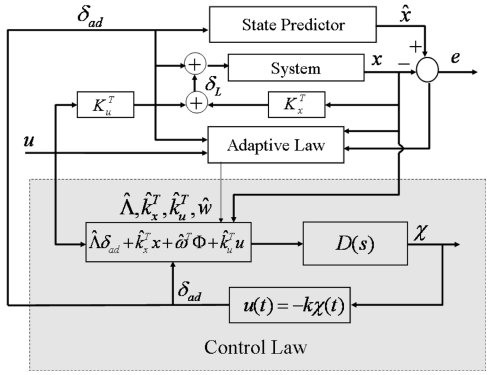

Fig. 4 Closed-loop system with $\mathcal{L}_1$ neural adaptive controller.

$$\gamma_{0_i} = \sqrt{\frac{\lambda_{\max}(P)}{\lambda_{\min}(P)}\left(\frac{2\|P\mathcal{B}_i\|}{\lambda_{\min}(Q_i)}(\epsilon_i^*)\right)^2 + \frac{W_{\max_i}}{\lambda_{\min}(P)\Gamma}} \qquad W_{\max_i} \triangleq \max_{W_i \in \Theta} 4\|W_i\|^2 \tag{29}$$

$$\gamma_{1_i} = \frac{5\epsilon_i^*\|\bar{G}_i(s)\|_{\mathcal{L}_1} + \|H_{o_i}(s)\|_{\mathcal{L}_1}\epsilon_i^* + (1 + \|C_i(s) - 1\|_{\mathcal{L}_1})\gamma_{0_i}}{1 - \|\bar{G}_i(s)\|_{\mathcal{L}_1} L} \tag{30}$$

where

$$H_{m_i}(s) \triangleq (s\mathbb{I} - A_{m_i})^{-1} B_{m_i} \tag{31}$$

$$H_{o_i}(s) \triangleq (s\mathbb{I} - A_{m_i})^{-1} \mathcal{B}_i \tag{32}$$

$$W_i^\top \triangleq \begin{bmatrix} \Lambda_i & k_{x_i}^\top & w_i^\top \end{bmatrix} \tag{33}$$

and Θ_i is the compact set to which W_i belongs. The complete $\mathcal{L}_1$ neural adaptive controller consists of Eqs. (11) and (17–19) subject to Eq. (24), with $\mathcal{D}_i$ defined in Eq. (27). The closed-loop system with it is illustrated in Fig. 4. To make the plot concise, the indices are omitted.

V. Analysis of the $\mathcal{L}_1$ Adaptive Controller

A. Closed-Loop Reference System

We now consider the following reference system, with its control signal and system response being defined as follows:

$$\dot{x}_{\text{ref}_i}(t) = A_{m_i} x_{\text{ref}_i}(t) + B_{m_i}\mathcal{R}_i(t) + \mathcal{B}_i\Big\{\Lambda_i u_{\text{ref}_i}(t) + k_{x_i}^\top x_{\text{ref}_i}(t) + w_i^\top \Phi_i[Y_{\text{ref}_i}(t)] + \epsilon_i[Y_{\text{ref}_i}(t)]\Big\} \tag{34}$$

$$u_{\text{ref}_i}(s) = \Lambda_i^{-1} C_i(s)\eta_{1_i}(s), \qquad x_{\text{ref}_i}(0) = x_{0_i} \tag{35}$$

where $\eta_{1_i}(s)$ is the Laplace transformation of the signal:

$$\eta_{1_i}(t) = -k_{x_i}^\top x_{\text{ref}_i}(t) + w_i^\top(t)\Phi_i[Y_{\text{ref}_i}(t)]$$

The control law in Eq. (35) leads to the following closed-loop dynamics:

$$x_{\text{ref}_i}(s) = H_{m_i}(s)\mathcal{R}_i(s) + \bar{G}_i(s)\eta_{1_i}(s) + H_{o_i}(s)\epsilon_i(s) \qquad y_{\text{ref}_i}(s) = c_i^\top x_{\text{ref}_i}(s), \qquad x_{\text{ref}}(0) = x_0 \tag{36}$$

where $\mathcal{R}_i(s)$, $\epsilon_i(s)$, and $\eta_{1_i}(s)$ are the Laplace transformations of the signals $\mathcal{R}_i(t)$, $\epsilon_i[x_{\text{ref}_i}(t)]$, and $\eta_{1_i}(t)$, respectively. The next Lemma establishes stability of the closed-loop system in Eqs. (34) and (35).

Lemma 1: The control signal given by Eq. (35), subject to the condition in Eq. (24), ensures that the state of the closed-loop system in Eq. (34) remains inside $\mathcal{D}_i$ for all $t \geq 0$; that is,

$$\|x_{\text{ref}_i}\|_{\mathcal{L}_\infty} \leq \gamma_{r_i} \tag{37}$$

where γ_{r_i} is defined in Eq. (28).

The proof can be found in [34].

B. Guaranteed Transient Performance of the $\mathcal{L}_1$ Neural Network Adaptive Controller

Let

$$B_{r_i} \triangleq [\mathcal{B}_i \bar{B}_i], \qquad H_{r_i}(s) \triangleq (s\mathbb{I} - A_{m_i})^{-1} B_{r_i} \qquad C_{r_i}(s) \triangleq \begin{bmatrix} C_i(s) & 0 \\ 0 & \bar{C}(s) \end{bmatrix} \tag{38}$$

where the choice of $\bar{B}_i$ renders B_{r_i} full rank with an appropriate dimension for each subsystem, and $\bar{C}(s)$ is an arbitrary diagonal strictly proper transfer function. The performance of the $\mathcal{L}_1$ adaptive neural controller is stated in the following Theorem.

Theorem 1: Given the system in Eq. (13), the reference system in Eqs. (34) and (35), and the $\mathcal{L}_1$ neural network adaptive controller defined via Eqs. (11) and (17–19) subject to Eq. (24), we have

$$\|x_i - \hat{x}_i\|_{\mathcal{L}_\infty} \leq \gamma_{0_i} \tag{39}$$

$$\|x_i - x_{\text{ref}_i}\|_{\mathcal{L}_\infty} \leq \gamma_{1_i} \tag{40}$$

$$\|u_{\text{ad}_i} - u_{\text{ref}_i}\|_{\mathcal{L}_\infty} \leq \gamma_{2_i} \tag{41}$$

where

$$\gamma_{2_i} = \|\Lambda_i^{-1} C_i(s)\|_{\mathcal{L}_1} L_i \gamma_{1_i} + \|\Lambda_i^{-1} C_{r_i}(s) H_{r_i}^{-1}(s)\|_{\mathcal{L}_1}[\gamma_{0_i} + \|H_{o_i}(s)\|_{\mathcal{L}_1}\epsilon_i^*] \tag{42}$$

The proof is in [34].

Remark 1: From the relationships in Eqs. (37) and (40), it is straightforward to verify that

$$\|x_i\|_{L_\infty} \leq \gamma_{r_i} + \gamma_{1_i}$$

and hence $x_i(t)$ belongs to $\mathcal{D}_i$ for any $t \geq 0$.

Corollary 1: Given the system in Eq. (13) and the $\mathcal{L}_1$ neural network adaptive controller defined via Eqs. (11) and (17–19) subject to Eq. (24), we have

$$\lim_{\Gamma \to \infty, \epsilon_i^* \to 0}[x_i(t) - \hat{x}_i(t)] = 0 \quad \forall\ t \geq 0$$

$$\lim_{\Gamma \to \infty, \epsilon_i^* \to 0}[x_i(t) - x_{\text{ref}_i}(t)] = 0 \quad \forall\ t \geq 0$$

$$\lim_{\Gamma \to \infty, \epsilon_i^* \to 0}[u_{\text{ad}_i}(t) - u_{\text{ref}_i}(t)] = 0 \quad \forall\ t \geq 0$$

Hence, if the approximation error of the RBF network is small enough, one can arbitrarily minimize the bounds between the signals of the closed-loop $\mathcal{L}_1$ adaptive system and the closed-loop reference system. Thus, the problem is reduced to the design of $C_i(s)$ to ensure that the closed-loop reference system approximates the response in Eq. (12). We note that the control law $u_{\text{ref}_i}(t)$ in the closed-loop reference system, which is used in the analysis of $\mathcal{L}_\infty$ norm bounds, is not implementable because its definition involves the unknown parameters. Theorem 1 ensures that the $\mathcal{L}_1$ adaptive controller approximates $u_{\text{ref}_i}(t)$ in both transient and steady states. So it is important to understand how these bounds can be used for ensuring uniform transient response with *desired* specifications. We notice that the following *ideal* control signal $u_{\text{ideal}}(t) = \Lambda_i^{-1}\eta_{1_i}(t)$ is the one that cancels the uncertainties exactly leading to Eq. (12), provided the neural network approximation is accurate enough. In

the closed-loop reference system (34), $u_{\text{ideal}}(t)$ is further low-pass filtered by $C_i(s)$ to have a guaranteed low-frequency range. In [27], specific design guidelines are provided for selection of $C_i(s)$ to ensure that reference system (34) tracks the response of the desired system in Eq. (12). One way to achieve this is via the selection of a strictly proper system $C_i(s)$ that minimizes the $\mathcal{L}_1$ gain of one of the cascaded system $C_i(s)[1 - C_i(s)]$. We also notice that for any finite L_i, condition (24) can always be satisfied by increasing the bandwidth of $C_i(s)$. However, as the analysis in [27] shows, increasing the bandwidth of $C_i(s)$ will lead to reduced time-delay margin.

Remark 2: Notice that setting $k_i \to \infty$ implies that the $\mathcal{L}_1$ neural controller reduces to the conventional MRAC-type architecture. Indeed, in this case, the adaptive control signal is being filtered with an infinite low-pass bandwidth, and therefore $u_{\text{ad}_i} \approx \bar{r}_i$. In that case,

$$\left\| \Lambda_i^{-1} C_{r_i}(s) H_{r_i}^{-1}(s) \right\|_{\mathcal{L}_1}$$

cannot be finite for any $i = 1, 2, 3$, because $H_{r_i}(s)$ is strictly proper. Therefore, from Eq. (42), it follows that $\gamma_{2_i} \to \infty$, and hence for the control signal in the conventional MRAC type neural network adaptive controller one cannot reduce the bound γ_{2_i} in Eq. (41) by increasing the adaptive gain.

Remark 3: Recall that in the conventional MRAC scheme the ultimate bound is given by γ_{0_i} defined in Eq. (29). Notice that γ_{0_i} depends upon ϵ_i^*, $W_{\max_i}$, and Γ. Although ϵ_i^* and $W_{\max_i}$ are interconnected via the choice of RBFs, Γ is a design parameter of the adaptive process that can be used to reduce the ultimate bound. However, increasing Γ in the conventional MRAC scheme leads the control signal into high-frequency oscillations. With the $\mathcal{L}_1$ adaptive control architecture, the ultimate bound of the tracking error is given by γ_{1_i} in Eq. (40). From the definition of it in Eq. (30), it follows that $\gamma_{1_i} > \gamma_{0_i}$. Nevertheless, the ability of the $\mathcal{L}_1$ control architecture to tolerate large adaptive gain implies that γ_{0_i} can be reduced, leading to an overall smaller value for γ_{1_i}. This is enabled via the low-pass system $C_i(s)$ in the feedback path that filters out the high frequencies in $\bar{r}_i(t)$ excited by large Γ. The $\mathcal{L}_1$ adaptive control architecture gives a scheme for fast adaptation without generating high-frequency oscillations in the control signal.

VI. Simulations

A 6-DOF model of the UAV (BANTAM) is used in the simulation. The tanker aircraft is in steady level flight. The target point for the receiver aircraft is chosen to be the center of the outer cross section of the drogue. The aircraft is trimmed at $V_0 = 500$ ft/s, $\alpha_0 = 0.042$ rad, $\theta_0 = 0.042$ rad, and at the altitude of $h = 5000$ ft. The radius of the drogue is $r_d = 1$ ft. The initial position of the receiver aircraft is 165 ft behind the tanker, 50 ft below the tanker, and 10 ft to the left of the aircraft laterally. Relative to the tanker coordinate system, the position of the drogue center is at the coordinates $x_d = -15$ ft, $y_d = 30$ ft, and $z_d = 10$ ft. The gains of the inner-loop controller are

$$K\text{lon}_{\text{in}} = \begin{bmatrix} -0.0261 & -1.9085 & -0.5462 & -1.8888 \\ 3 & 0 & 0 & 0 \end{bmatrix}$$
$$K\text{lat}_{\text{in}} = \begin{bmatrix} 0.0072 & 0 & 0.0069 & 0 \\ 0 & 0.9356 & 0 & -0.6815 \end{bmatrix} \tag{43}$$

where $K\text{lon}_{\text{in}}$ is applied to longitudinal dynamics, for which the states are $[u \;\; \alpha \;\; \theta \;\; q]^\top$ and controls are $[\delta_e \;\; \delta_T]^\top$, and $K\text{lat}_{\text{in}}$ is applied to lateral dynamics, for which the states are $[\phi \;\; \beta \;\; p \;\; s]^\top$ and controls are $[\delta_a \;\; \delta_r]^\top$. The gains of the outer-loop LQR and the integral controller are

$$K_1 = -[215.5238 \;\; 410.1226 \;\; 54.7723]$$
$$K_2 = -[0.0934 \;\; 1.5425 \;\; 1.3772 \;\; 0.3695 \;\; -0.0667 \;\; -0.0141]$$
$$K_3 = -[0.0114 \;\; 0.7592 \;\; 0.0307 \;\; -0.2561 \;\; 0.0861 \;\; 0.0141] \tag{44}$$

These control gains are applied to the linearized aircraft model, with A and B given as follows:

$$A = \begin{bmatrix} 0 & 1.0 & 0 & 0 & 0 & 0 & 0 & 0 & 0 & 0 & 0 \\ 0 & -0.03 & -6.4 & -32.1 & -24.8 & -5e-4 & 0 & 0 & 0 & 0 & 0 \\ 0 & 2e-4 & -0.94 & -3.2e-3 & 0.98 & 0 & 0 & 0 & 0 & 0 & 0 \\ 0 & 0 & 0 & 0 & 1 & 0 & 0 & 0 & 0 & 0 & 0 \\ 0 & 0.04 & 37.8 & 0 & -2.7 & 8e-4 & 0 & 0 & 0 & 0 & 0 \\ 0 & -0.05 & 498.8 & -500 & 0 & 0 & 0 & 0 & 0 & 0 & 0 \\ 0 & 0 & 0 & 0 & 0 & 0 & 0 & 0 & 1 & 0.05 & 0 \\ 0 & 0 & 0 & 0 & 0 & 0 & 0.06 & -0.02 & 0.05 & -1 & 0 \\ 0 & 0 & 0 & 0 & 0 & 0 & 0 & -9.7 & -2.1 & 0.16 & 0 \\ 0 & 0 & 0 & 0 & 0 & 0 & 0 & -2.6 & -0.1 & -0.01 & 0 \\ 0 & 0 & 0 & 0 & 0 & 0 & -24.6 & 500 & 0 & 0 & 0 \end{bmatrix} \tag{45}$$

$$B = \begin{bmatrix} 0 & 0.17 & -0.0029 & 0 & -0.4 & 0 & 0 & 0 & 0 & 0 & 0 \\ 0 & 0.0024 & 0 & 0 & 0 & 0 & 0 & 0 & 0 & 0 & 0 \\ 0 & 0 & 0 & 0 & 0 & 0 & 0 & -0.0002 & 0.3 & 0.017 & 0 \\ 0 & 0 & 0 & 0 & 0 & 0 & 0 & -0.0001 & 0.061 & -0.064 & 0 \end{bmatrix}^\top \tag{46}$$

The closed-loop system with these baseline controller gains defines the nominal linear system response that has the desired convergence time for the probe to contact the drogue with desired performance specifications. The adaptive augmentation with the $\mathcal{L}_1$ controller is designed to track this system's response in both transient and steady states. With the specified baseline controller gains, in the absence of wake-induced uncertainties and without any loss in control effectiveness, the probe reaches to the 0.02-ft neighborhood of the drogue center within 25 s. That is, $|x(25) - x_d(25)| = 0.012$, $|y(25) - y_d(25)| = 0.015$, and $|z(25) - z_d(25)| = 0.02$. Figure 5 plots the closed-loop trajectories in each axis. It compares the

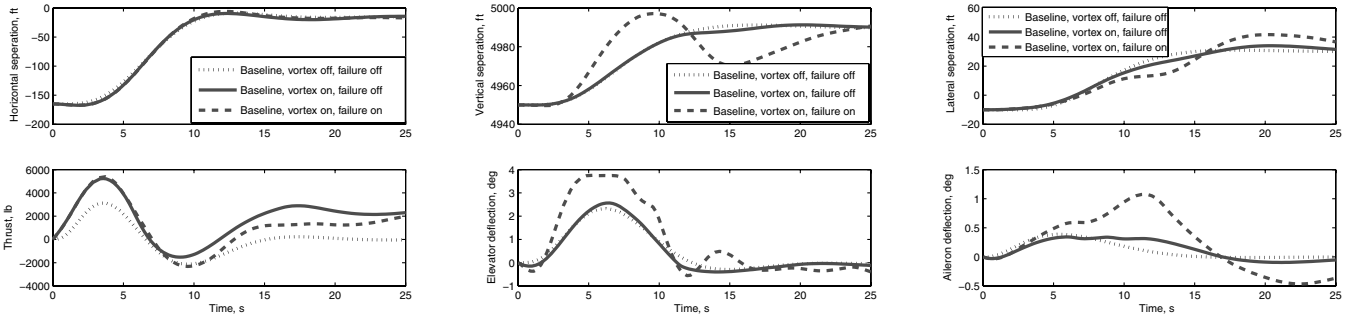

Fig. 5 Horizontal, vertical, and lateral separation; baseline controller.

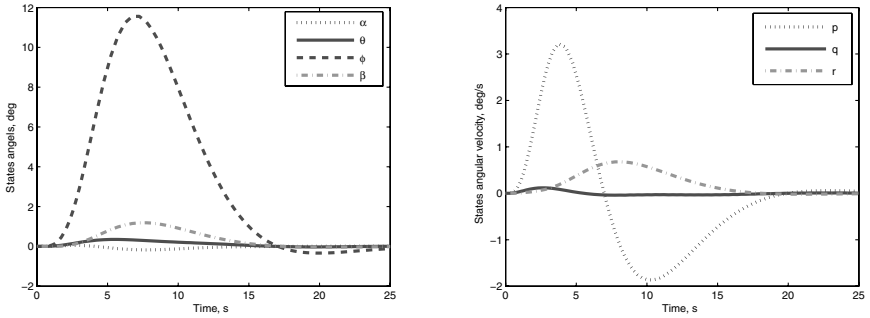

Fig. 6 Angles and angular velocities; baseline controller.

responses in the absence of the wake and without any loss in control effectiveness with that in the presence of the wake and loss in control effectiveness. The failures are 60% reduction of elevator effectiveness and 60% reduction of aileron effectiveness; that is, $\Lambda_2 = \Lambda_3 = 0.4$. From these figures, we can see that both the steady-state tracking and the transient performance are deteriorated in the presence of uncertainties. Figure 6 shows the other states (α, θ, ϕ, β, p, q, r) of the baseline-controlled closed-loop system. Those states remain small during the whole aerial refueling process.

For the design of the $\mathcal{L}_1$ controller we choose $D(s) = 1/s$. Next, we calculate the $\|\bar{G}_i(s)\|_{\mathcal{L}_1}$ numerically as a function of k_i and compare it with the inverse of L_i. Conservative growth rates for the uncertainties are computed from the experimental data, implying that $\max L_{w_i} = 0.1$. In Fig. 5, the effect of the uncertainties on the system's performance is shown. Then we calculate the bounds on k_{x_i} as $L_{x_1} = 0$, $L_{x_2} = 10$, and $L_{x_3} = 10$. Hence, the conservative maximum is $L_i = 10.1$. From Fig. 7, we can choose $k_1 = k_2 = k_3 = 15$, leading to $C_1(s) = 15/(s + 15)$, $C_2(s) = 6/(s + 6)$, and $C_3(s) = 6/(s + 6)$. Nine RBFs were selected for the implementation of the adaptive controller in each channel. The choice of the low-pass filter satisfies the stability requirement $\|\bar{G}_i(s)\|_{\mathcal{L}_1} L_i < 1$. We set a uniform adaptive gain $\Gamma = 10,000$ for the design of the adaptive controller in each axis. The closed-loop system response with $\mathcal{L}_1$ adaptive augmentation is shown in Fig. 8.

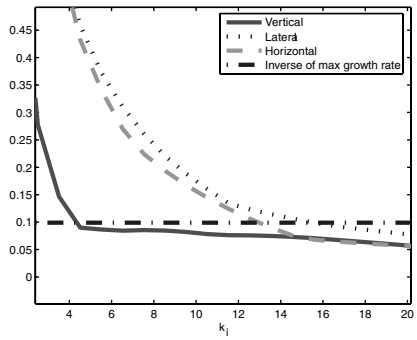

Fig. 7 Comparison between $\|\bar{G}_i(s)\|_{\mathcal{L}_1}$ and the growth rate.

To explicitly show the benefits of $\mathcal{L}_1$ adaptive controller, we compare its responses with those of the MRAC architecture. Here, we introduce the MRAC briefly. We start from the partially closed-loop system (13), and consider a reference model instead of the predictor model:

$$\dot{x}_m(t) = A_{m_i} x_m(t) + B_{m_i} \mathcal{R}_i(t) \tag{47}$$

The adaptive input in Eq. (13) for MRAC is given by

$$u_{\mathrm{ad}_i}(t) = \hat{k}_{x_i}^{\top}(t) x_i(t) + \hat{w}_i^{\top}(t) \Phi(Y) \tag{48}$$

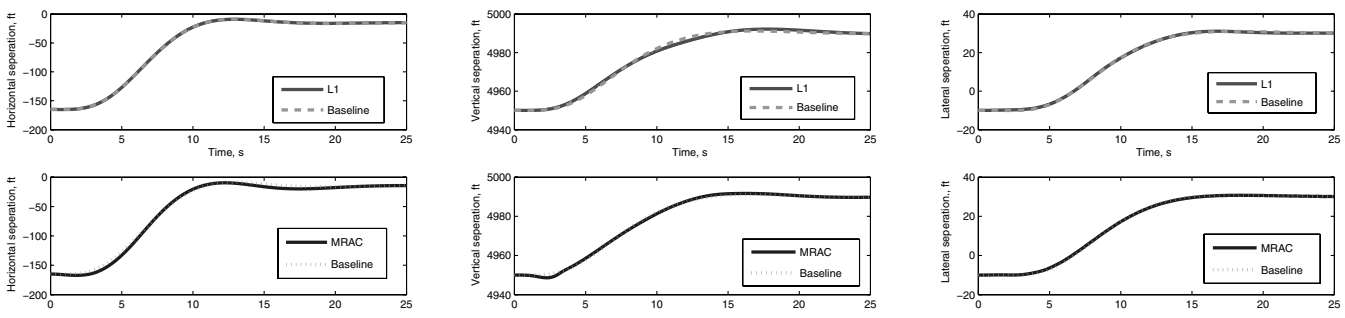

Fig. 8 Horizontal, vertical, and lateral separation; baseline and $\mathcal{L}_1$ controller.

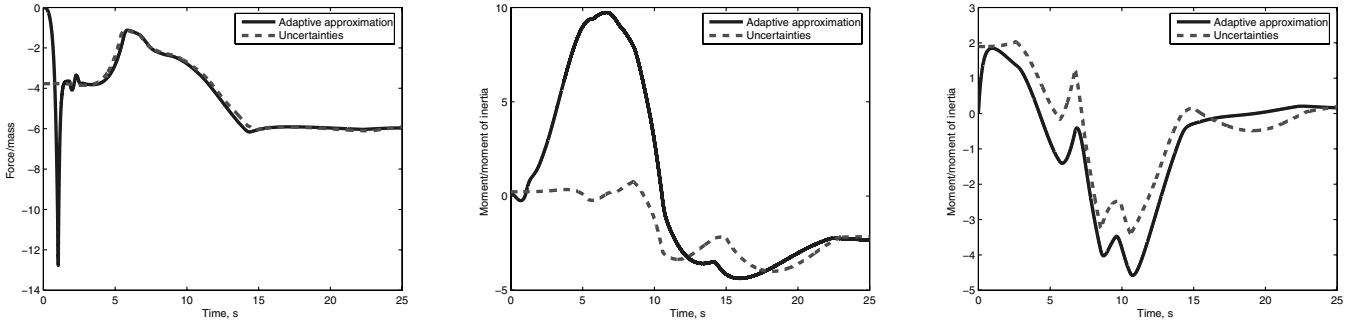

Fig. 9 $\mathcal{L}_1$ adaptive control signals and uncertainties.

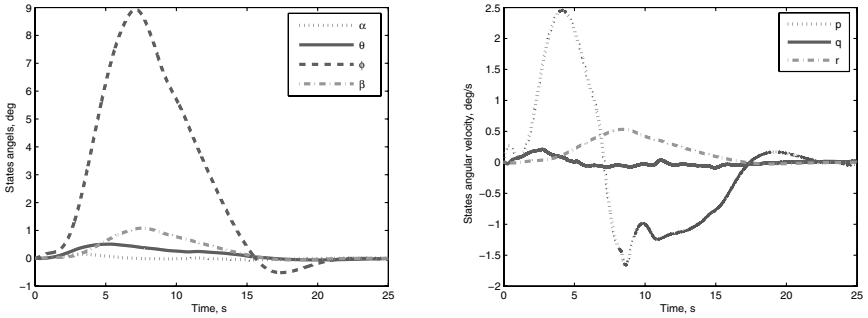

Fig. 10 Angles and angular velocities; $\mathcal{L}_1$ controller.

where the parameters $\hat{k}_{x_i}(t)$ and $\hat{w}_i(t)$ can be obtained from the same adaptive law (18), replacing $\tilde{x}(t) = \hat{x}(t) - x(t)$ by $\tilde{x}(t) = x_m(t) - x(t)$. In Fig. 8, MRAC is tuned to have satisfactory performance. In Figs. 9 and 10, $\mathcal{L}_1$ adaptive control signals and the states of the adaptively controlled closed-loop system are shown. We notice that both $\mathcal{L}_1$ and MRAC adaptive controllers can recover the nominal performance of the baseline controller in the presence of the wake vortex and loss in control effectiveness. The tracking precision upon $t' = 25$ s can be characterized with the bound

$$\|[y(t') \;\; z(t')]^\top - [y_d(t') \;\; z_d(t')]^\top\| = 0.05 \leq 1$$

and $|x(t') - x_d(t')| = 0.04$. Next, we show that when the initial conditions change, the $\mathcal{L}_1$ controller does not need any retuning.

We change the initial conditions of the receiver. We keep the same values for Λ_1 and Λ_2 and run the simulations from 33.75 ft behind the tanker, 18 ft below the tanker, and 22 ft to the right of the tanker, without any retuning of both controllers. The $\mathcal{L}_1$ adaptive controller achieves the tracking precision upon $t' = 25$ s, which is

$$\|[y(t') \;\; z(t')]^\top - [y_d(t') \;\; z_d(t')]^\top\| = 0.021 \leq 1$$

and $|x(t') - x_d(t')| = 0.020$, as in Fig. 11. We observe that MRAC cannot recover the previous performance without retuning of the adaptation gains, whereas the $\mathcal{L}_1$ adaptive controller shows scaled system output responses (similar to linear systems).

Without retuning of the $\mathcal{L}_1$ controller, we further run the simulation starting from various different initial conditions, as shown in Fig. 12. It can be seen that the system outputs have scaled responses. We further increase the uncertainties by multiplying the magnitude of the vortex data by two. This can approximately represent a different tanker if we consider a modified horseshoe-vortex model [15]. With fixed separations between the receiver and the tanker, the magnitude of the induced velocity is proportional to the strength of the vortex, which is in turn proportional to the mean aerodynamic chord of the tanker and velocity of the tanker. So it is reasonable to scale our current induced aerodynamic coefficients by multiplying them by two to represent the change of the tanker's wake effects. Figure 13 show that the outputs are identical to the nominal performance, and Fig. 14 shows that the adaptive control signals have scaled responses corresponding to the change of uncertainties.

VII. Conclusions

A novel $\mathcal{L}_1$ adaptive neural network controller is presented in this paper for autonomous aerial refueling autopilot design. The method has a systematic design theory to achieve uniform smooth transient performance for the system's signals, both inputs and outputs, simultaneously. By increasing the adaptation rate, all the signals of the closed-loop adaptive system track the same signals of a corresponding reference system in both the transient and steady states. Simulations of a tailless unstable 6-DOF model of BANTAM have verified the theoretical findings.

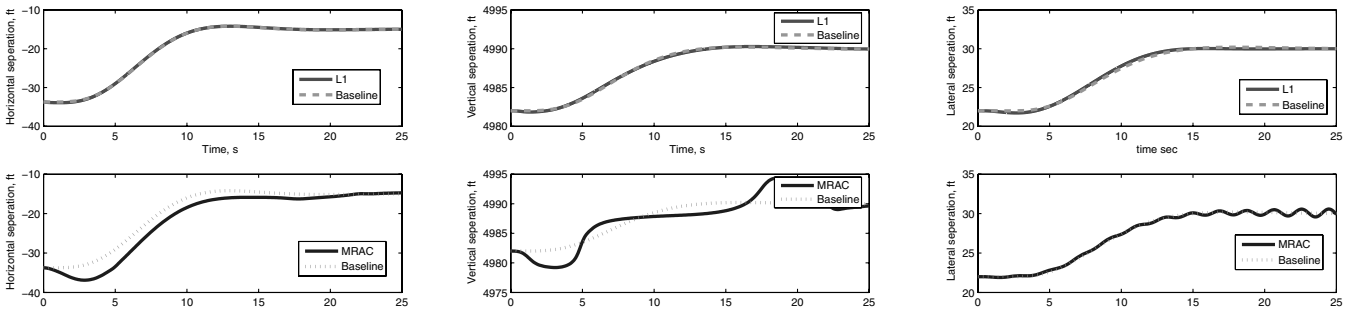

Fig. 11 Horizontal, vertical, and lateral separation; second case.

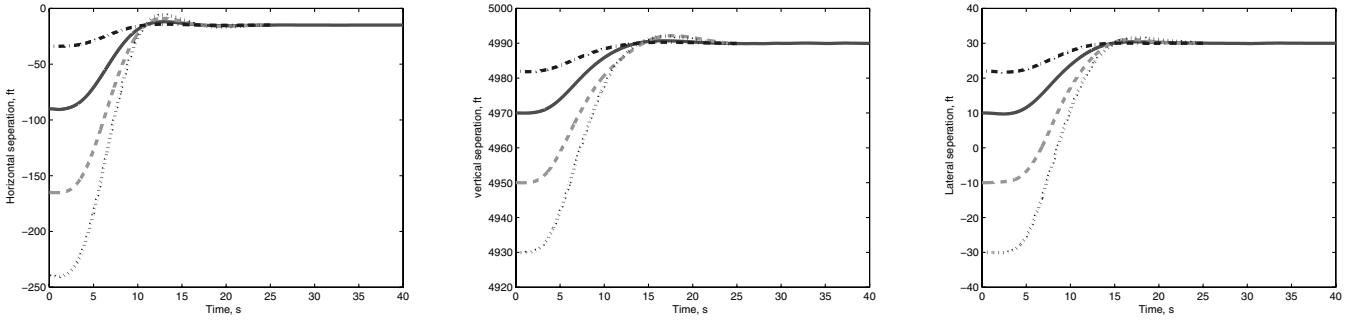

Fig. 12 Horizontal, vertical, and lateral separation; scaled responses.

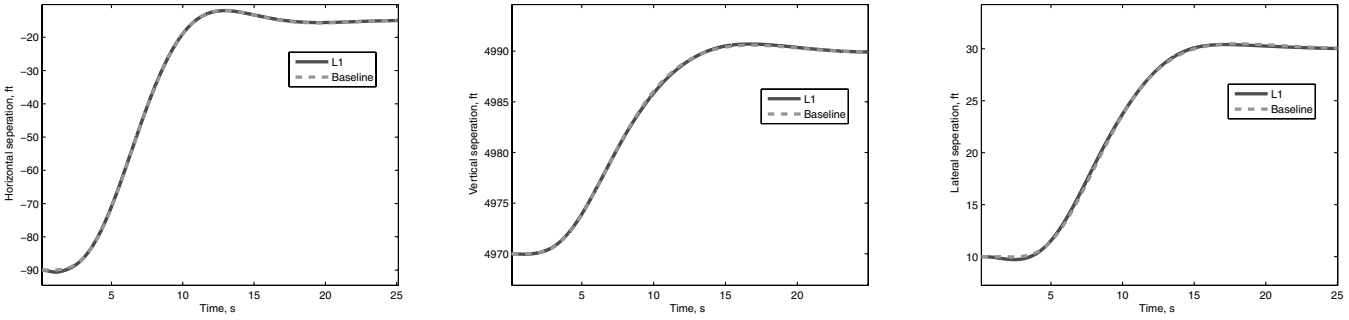

Fig. 13 Horizontal, vertical, and lateral separation; increased vortex magnitude.

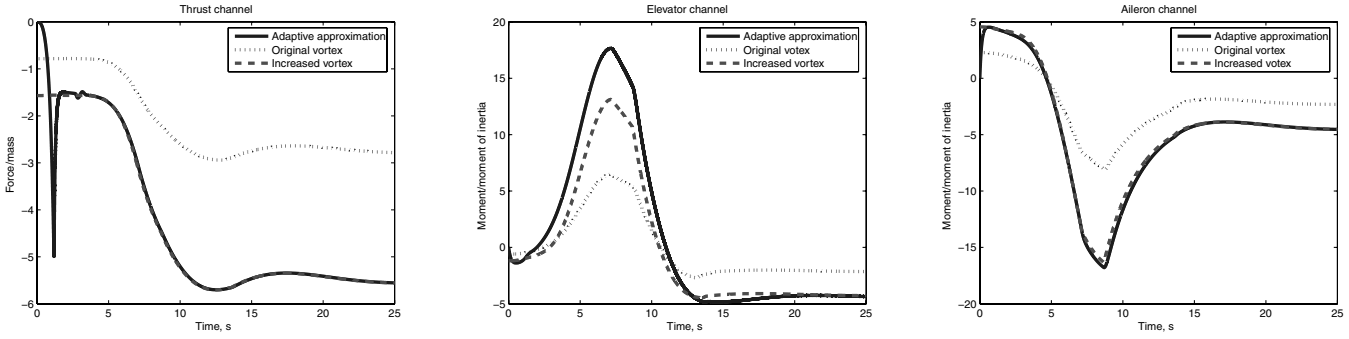

Fig. 14 Adaptive signals vs uncertainties; increased vortex magnitude.

Appendix: Projection Operator

The projection operator introduced in [33] ensures boundedness of the parameter estimates by definition. We recall the main definition from [33]:

Definition 1: Consider a convex compact set with a smooth boundary given by

$$\Omega_c \Delta = \{\boldsymbol{\theta} \in \mathbb{R}^n \mid f(\boldsymbol{\theta}) \leq c\}, \qquad 0 \leq c \leq 1 \tag{A1}$$

where f: $\mathbb{R}^n \to \mathbb{R}$ is the following smooth convex function:

$$f(\boldsymbol{\theta}) = \frac{\boldsymbol{\theta}^\top \boldsymbol{\theta} - \theta_{\max}^2}{\epsilon_\theta} \tag{A2}$$

where $\theta_{\max} > 0$ is the norm bound imposed on the parameter vector $\boldsymbol{\theta}$, and $0 < \epsilon_\theta < 1$ denotes the convergence tolerance of our choice. For any given $\mathbf{y} \in \mathbb{R}^n$, the projection operator is defined as

$$\text{proj}\,(\boldsymbol{\theta}, \boldsymbol{y}) = \begin{cases} \boldsymbol{y}, & \text{if } f(\boldsymbol{\theta}) < 0 \\ \boldsymbol{y}, & \text{if } f(\boldsymbol{\theta}) \geq 0, \nabla f^\top \boldsymbol{y} \leq 0 \\ \boldsymbol{y} - \boldsymbol{g}(f, \boldsymbol{y}), & \text{if } f(\boldsymbol{\theta}) \geq 0, \nabla f^\top \boldsymbol{y} > 0 \end{cases}$$

where

$$\boldsymbol{g}\,(f, \boldsymbol{y}) = \frac{\nabla f \nabla f^\top \boldsymbol{y}}{\|\nabla f\|^2} f(\boldsymbol{\theta}) \tag{A3}$$

The properties of the projection operator are given by the following Lemma:

Lemma 2: Let

$$\boldsymbol{\theta}^* \in \Omega_0 = \{\boldsymbol{\theta} \in \mathbb{R}^n \mid f(\boldsymbol{\theta}) \leq 0\}$$

and let the parameter $\boldsymbol{\theta}(t)$ evolve according to the following dynamics:

$$\dot{\boldsymbol{\theta}}(t) = \text{proj}[\boldsymbol{\theta}(t), \boldsymbol{y}], \qquad \boldsymbol{\theta}(t_0) \in \Omega_c \tag{A4}$$

Then

$$\boldsymbol{\theta}\,(t) \in \Omega_c \tag{A5}$$

for all $t \geq t_0$, and

$$h_{\boldsymbol{\theta}, \boldsymbol{y}} \triangleq [\boldsymbol{\theta}(t) - \boldsymbol{\theta}^*]^\top \{\text{proj}[\boldsymbol{\theta}(t), \boldsymbol{y}] - \boldsymbol{y}\} \leq 0 \tag{A6}$$

From Definition 1, it follows that $\boldsymbol{y}$ is not altered if $\boldsymbol{\theta}$ belongs to the set Ω_0. In the set $\{0 \leq f(\boldsymbol{\theta}) \leq 1\}$, $\text{proj}(\boldsymbol{\theta}, \boldsymbol{y})$ subtracts a vector normal to the boundary of Ω_c so that we get a smooth transformation from the original vector field $\boldsymbol{y}$ to an inward or tangent vector field for

$c = 1$. Therefore, on the boundary of Ω_c, $\dot{\boldsymbol{\theta}}(t)$ always points toward the inside of Ω_c and $\boldsymbol{\theta}(t)$ never leaves the set Ω_c, which is the first property.

From the convexity of function $f(\boldsymbol{\theta})$, it follows that for any $\boldsymbol{\theta}^* \in \Omega_0$ and $\boldsymbol{\theta} \in \Omega_c$, the inequality

$$l_{\boldsymbol{\theta}} \triangleq (\boldsymbol{\theta} - \boldsymbol{\theta}^*)^\top \nabla f(\boldsymbol{\theta}) \leq 0$$

holds. Then from Definition 1, it follows that

$$h_{\boldsymbol{\theta},\boldsymbol{y}} = \begin{cases} 0, & \text{if } f < 0 \\ 0, & \text{if } f \geq 0, \nabla f^\top \boldsymbol{y} \leq 0 \\ \dfrac{\underbrace{l}_{\leq 0}\ \underbrace{\nabla f^T \boldsymbol{y}}_{\geq 0}\ \underbrace{f(\boldsymbol{\theta})}_{\geq 0}}{\|\nabla f\|^2}, & \text{if } f \geq 0, \nabla f^\top \boldsymbol{y} > 0 \end{cases}$$

This shows the second property.

Acknowledgment

This material is based upon work supported by the U.S. Air Force under contracts FA8650-05-C-3563, FA9550-05-1-0157, and FA9550-04-C-0047 and the Office of Naval Research (ONR) under contract N00014-05-1-0828. Any opinions, findings, conclusions, or recommendations expressed in this material are those of the authors and do not necessarily reflect the views of the U.S. Air Force or the ONR. The authors are thankful to Manu Sharma for providing the 6-DOF simulator model for this problem. Many useful discussions with him were helpful toward the development of the results in this paper.

References

[1] Nalepka, J. P., and Hinchman, J. L., "Automated Aerial Refueling: Extending the Effectiveness of Unmanned Air Vehicles," AIAA Modeling and Simulation Technologies Conference and Exhibit, San Francisco, AIAA Paper 2005-6005, Aug. 2005.

[2] Abidi, M. A., and Gonzalez, R. C., "The Use of Multisensor Data for Robotic Applications," *IEEE Transactions on Robotics and Automation*, Vol. 6, No. 2, 1990, pp. 159–177. doi:10.1109/70.54732

[3] Andersen, C. M., "Three Degrees of Freedom Compliant Motion Control for Robotic Aircraft Refueling," U.S. Air Force Inst. of Technology, Rept. AD-A230581, Wright–Patterson AFB, OH, Dec. 1990.

[4] Bennett, R. A., "Brightness Invariant Port Recognition for Robotic Aircraft Refueling," U.S. Air Force Inst. of Technology, Rept. Afit/gae/eng/90d-04, Wright–Patterson AFB, OH, 13 Dec. 1990.

[5] Blake, W. B., Dickes, E. G., and Gingras, D. R., "UAV Aerial Refueling —Wind Tunnel Results and Comparison with Analytical Predictions," AIAA Atmospheric Flight Mechanics Conference and Exhibit, Providence, RI, AIAA Paper 2004-4820, 2004.

[6] Dogan, A., Sato, S., and Blake, W., "Flight Control and Simulation for Aerial Refueling," AIAA Guidance, Navigation, and Control Conference and Exhibit, San Francisco, AIAA Paper 2005-6264, 2005.

[7] Campa, G., Fravolini, M. L., Ficola, A., Napolitano, M. R., Seanor, B., and Perhinschi, M. G., "Autonomous Aerial Refueling for UAVs Using a Combined GPS-Machine Vision Guidance," AIAA Guidance, Navigation, and Control Conference and Exhibit, Providence, RI, AIAA Paper 2004-5350, Aug. 2004.

[8] Fravolini, M. L., Ficola, A., Napolitano, M. R., Campa, G., and Perhinschi, M. G., "Development of Modelling and Control Tools for Aerial Refueling for UAV," AIAA Guidance, Navigation, and Control Conference, Austin, TX, AIAA Paper 2003-5798, 2003.

[9] Lachapelle, G., Sun, H., Cannon, M. E., and Lu, G., "Precise Aircraft-to-Aircraft Positioning Using a Multiple Receiver Configuration," *National Technical Meeting*, Inst. of Navigation, San Diego, CA, 1994, pp. 793–799.

[10] Pachter, M., Houpis, C., and Trosen, D., "Design of an Air-to-Air Automatic Refueling Flight Control System Using Quantitative Feedback Theory," *International Journal of Robust and Nonlinear Control*, Vol. 7, No. 6, 1997, pp. 561–580. doi:10.1002/(SICI)1099-1239(199706)7:6<561::AID-RNC291>3.0.CO;2-V

[11] Shipman, R. P., "Visual Servoing for Autonomous Aircraft Refueling," U.S. Air Force Inst. of Technology, Rept. Afit/gae/eng/89d-48, Wright–Patterson AFB, OH, 13 Dec. 1989.

[12] Stepanyan, V., Lavretsky, E., and Hovakimyan, N., "Aerial Refueling Autopilot Design Methodology: Application to F-16 Aircraft Model," AIAA Guidance, Navigation, and Control Conference, Providence, RI, AIAA Paper 2004-5321, 2004.

[13] Valasek, J., Gunnam, K., Kimmett, J., Tandale, M. D., Junkins, J. L., and Hughes, D., "Vision-Based Sensor and Navigation System for Autonomous Air Refueling," *Journal of Guidance, Control, and Dynamics*, Vol. 28, No. 5, 2005, pp. 979–989.

[14] Tandale, M. D., Bowers, R., and Valasek, J., "Trajectory Tracking Controler for Vision-Based Probe and Drogue Autonomous Aerial Refueling," *Journal of Guidance, Control, and Dynamics*, Vol. 29, No. 4, 2006, pp. 846–857.

[15] Venkataramanan, S., Dogan, A., and Blake, W., "Vortex Effect Modelling in Aircraft Formation Flight," AIAA Atmospheric Flight Mechanics Conference and Exhibit, Austin, TX, AIAA Paper 2003-5385, 2003.

[16] Ross, S. M., Pachter, M., Jacques, D. R., Kish, B. A., and Millman, D. R., "Autonomous Aerial Refueling Based on the Tanker Reference Frame," 2006 IEEE Aerospace Conference, Big Sky, MT, Inst. of Electrical and Electronics Engineers, Piscataway, NJ, Mar. 2006. doi:10.1109/AERO.2006.1656016

[17] Smith, A. L., and Kunz, D. L., "Dynamic Coupling of the KC-135 Tanker and Boom for Modeling and Simulation," AIAA Modeling and Simulation Technologies Conference and Exhibit, Keystone, CO, AIAA Paper 2006-6480, Aug. 2006.

[18] Ochi, Y., and Kominami, T., "Flight Control for Automatic Aerial Refueling via PNG and LOS Angle Control," AIAA Guidance, Navigation, and Control Conference and Exhibit, San Francisco, AIAA Paper 2005-6268, Aug. 2005.

[19] Herrnberger, M., Sachs, G., Holzapfel, F., Tostmann, W., and Weixler, E., "Simulation Analysis of Autonomous Aerial Refueling Procedures," AIAA Guidance, Navigation, and Control Conference and Exhibit, San Francisco, AIAA Paper 2005-5866, Aug. 2005.

[20] Johnson, K., and Awni, K., "A Roll Autopilot for Autonomous Air Refueling," AIAA Guidance, Navigation, and Control Conference and Exhibit, Monterey, CA, AIAA Paper 2002-4752, Aug. 2002.

[21] Zang, Z., and Bitmead, R., "Transient Bounds for Adaptive Control Systems," *Proceedings of the 30th IEEE Conference on Decision and Control*, Inst. of Electrical and Electronics Engineers, Piscataway, NJ, Dec. 1990, pp. 2724–2729.

[22] Cao, C., and Hovakimyan, N., "Novel $\mathcal{L}_1$ Neural Network Adaptive Control Architecture with Guaranteed Transient Performance," *IEEE Transactions on Neural Networks*, Vol. 18, No. 4, July 2007, pp. 1160–1171. doi:10.1109/TNN.2007.899197

[23] Cao, C., and Hovakimyan, N., "Design and Analysis of a Novel $\mathcal{L}_1$ Adaptive Controller, Part 2: Control Signal and Asymptotic Stability," *American Control Conference*, Inst. of Electrical and Electronics Engineers, Piscataway, NJ, 2006, pp. 3397–3402.

[24] Cao, C., and Hovakimyan, N., "Design and Analysis of a Novel $\mathcal{L}_1$ Adaptive Controller, Part 2: Guaranteed Transient Performance," *American Control Conference*, Inst. of Electrical and Electronics Engineers, Piscataway, NJ, 2006, pp. 3403–3408.

[25] Wang, J., Cao, C., Hovakimyan, N., and Lavretsky, E., "Novel $\mathcal{L}_1$ Adaptive Control Approach to Autonomous Aerial Refueling with Guaranteed Transient Performance," *American Control Conference*, Inst. of Electrical and Electronics Engineers, Piscataway, NJ, 2006, pp. 3569–3574.

[26] Cao, C., and Hovakimyan, N., "Guaranteed Transient Performance with $\mathcal{L}_1$ Adaptive Controller for Systems with Unknown Time-Varying Parameters and Bounded Disturbance: Part 1," *American Control Conference*, Inst. of Electrical and Electronics Engineers, Piscataway, NJ, 2007, pp. 3925–3930.

[27] Cao, C., and Hovakimyan, N., "Stability Margins of $\mathcal{L}_1$ Adaptive Controller: Part 2," *American Control Conference*, Inst. of Electrical and Electronics Engineers, Piscataway, NJ, 2007, pp. 3931–3936.

[28] Cao, C., Patel, V., Reddy, C. K., Hovakimyan, N., and Lavretsky, E., "Are the Phase and Time-Delay Margins Always Adversely Affected by High-Gain?," AIAA Guidance, Navigation, and Control Conference, AIAA Paper 2006-6347, 2006.

[29] Wang, J., Patel, V. V., Cao, C., Hovakimyan, N., and Lavretsky, E., "$\mathcal{L}_1$ Adaptive Neural Network Controller for Autonomous Aerial Refueling with Guaranteed Transient Performance," AIAA Guidance, Navigation, and Control Conference, AIAA Paper 2006-6206, 2006.

[30] Stevens, B., and Lewis, F., *Aircraft Control and Simulation*, Wiley, New York, 1992.

[31] Farrell, J., Sharma, M., and Polycarpou, M., "Backstepping-Based

Flight Control with Adaptive Function Approximation," *Journal of Guidance, Control, and Dynamics*, Vol. 28, No. 6, 2005, pp. 1089–1102.

[32] Fears, S. P., Ross, H. M., and Moul, T. M., "Low-Speed Wind-Tunnel Investigation of the Stability and Control Characteristics of a Series of Flying Wings with Sweep Angles of 50°," NASA TM 4640, June 1995.

[33] Pomet, J., and Praly, L., "Adaptive Nonlinear Regulation: Estimation from the Lyapunov Equation," *IEEE Transactions on Automatic Control*, Vol. 37, No. 6, 1992, pp. 729–740. doi:10.1109/9.256328

[34] Patel, V. V., Cao, C., Hovakimyan, N., Wise, K. A., and Lavretsky, E., "$\mathcal{L}_1$ Adaptive Controller for Tailless Unstable Aircraft in the Presence of Unknown Actuator Failures," AIAA Guidance, Navigation, and Control Conference, AIAA Paper 2007-6314, 2007.